Nature of the bonding, surface relaxation and charge transfer of Au dimmers on an MgO(100) surface

C. Quintanar[a], R. Caballero[a], J. Ulises Reveles[b], and S.N. Khanna[b]
[a]*Facultad de Ciencias, Universidad Nacional Autónoma de México, Ciudad Universitaria, 04510 México, D.F., México.*
e-mail: cqs@matrix.super.unam.mx
[b]*Physics Department, Virginia Commonwealth University, Richmond, Virginia, 23284-2000, USA.*

Recibido el 12 de mayo de 2011; aceptado el 15 de diciembre de 2011

First principles electronic structure investigations of the nature of adsorption, relaxation of the atoms near the adsorption site, and the charging of the Au_2 particle on the relaxed-rumpled MgO(100) surface have been carried out within the density functional theory-cluster-embedding approach. The investigations focus on an Au_2 molecule, perpendicular to the surface, adsorbed at different locations. Three bonding sites are studied: a five coordinated oxygen regular terrace site O_{5c}, an F_s neutral color center (two electrons in an O vacancy), and an F_s^+ positive charged color center (one electron in an O vacancy). The studies indicate that large relaxation of the neighboring atoms and large charge transfer occurs for an Au_2 over the color centers. An analysis of the one-electron energy levels of the Au dimer, the MgO surface and the Au_2MgO(100) complex for each absorption site allows us to rationalize the nature of the bonding, surface relaxation, calculated absorption and dimerization energies and electron charge transfers.

Keywords: Supported gold nanoparticles; gold catalysis; density functional theory; metal oxides.

PACS: 61.72.Ji; 68.47.Jn

1. Introduction

In recent year there has been a sustained interest in supported gold nano-particles as catalysts for a very broad range of reactions [1-4]. Most interest has been focused in CO oxidation at ambient temperature; although, gold nano-particles supported on MgO can have some other applications, like to enhance the performance of protective layer alternating current plasma display panels [4].

Experimental and theoretical studies over the past several years have shown that the catalytic activity of small gold clusters supported on metal oxides surfaces, first discovered by Haruta *et al.* [5], depends on several factors; the size of the clusters [6-10], poorly coordinated gold atoms [2,7], the presence of defect centers in the underlying surface [6,12], and the electronic charge induced in the clusters via the interaction with the surface [6,13]. From all these factors, the low coordination of the gold atoms, and the properties of the Au-oxide interface are found to have the greatest influence on activity. Although some studies indicate that catalytically active free gold particles must have a specific size (of the order of few nanometers) [9-10], experimental studies on surface-supported Au_8 indicate that gold clusters on a defect-rich MgO surface are more active than on a defect-poor surface [6]. These results show that the supporting surface does play an important role. Haruta *et al.* [12] experimentally investigated the effects of support upon CO oxidation for Au catalysts irrespective of Au particle size, and concluded that the nature of the contact between the Au particle and the supporting surface is even more important than the particle size. Among the possible surface absorption sites, defect centers formed by oxygen vacancies in the surface of MgO in which one or two electrons are trapped (F_s^+ and F_s centers respectively) have attracted considerable attention. These sites facilitate cluster growth and promote catalytic activity by enhancing the charge transfer from the surface to the adsorbed cluster [14-15].

Several ab initio studies have been reported aimed at providing a detailed, atomic-level description of the catalytic reaction, and at quantifying the properties that contribute to the enhanced catalytic activity of the gold clusters [16-27]. In particular, several authors have done density functional theory (DFT) studies of the adsorption of Au_2 over the MgO(100) surface, and several isomers have been reported at the different adsorption sites [16,19,21-23,25,27].

In the present work we have carried out detailed investigation of one isomer that has been found to be common to all adsorption sites studied, namely the Au_2 dimer perpendicular to the MgO(100) surface, in order to compare the characteristics of the adsorption sites O_{5c}, F_s and F_s^+. Consequently, in this work we have studied the only Au_2 isomer common to these adsorption sites, specifically the dimer almost perpendicular to the MgO(100) surface.

The studies cover three adsorption sites: Au_2 over a five-coordinated regular oxygen site O_{5c}, and over surface defects, namely F_s (two electrons in an oxygen vacancy), and F_s^+ (one electron in an oxygen vacancy) color centers. Our investigations allows us to analyze the nature of bonding of the Au_2 dimer to the MgO(100) surface, to compare the contact-structure geometries of the same gold cluster adsorbed on different surface sites, and to study absorption and dimerization energies and the charge transfer from those surface sites to the gold dimer.

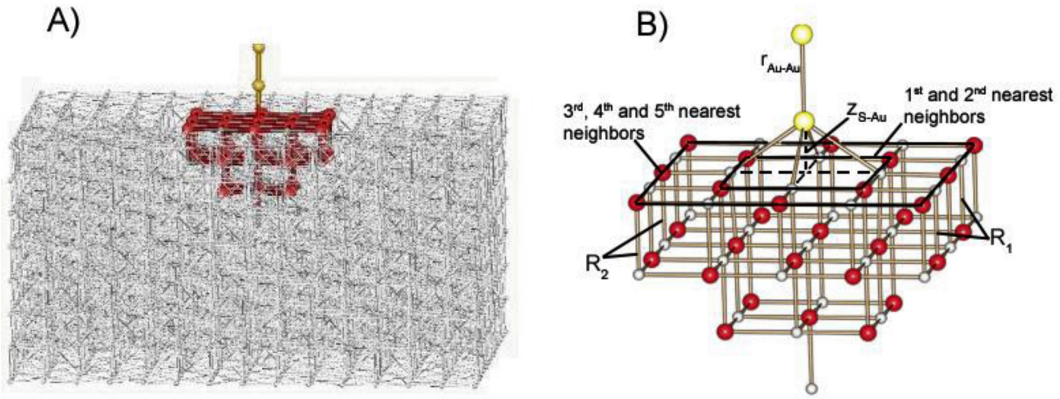

FIGURE 1. (A) Au_2 over an oxygen atom of an embedded $Mg_{30}O_{30}$ cluster. The cluster is centered at an oxygen site of the MgO(100) surface, and the embedding has 1740 point charges. (B) $Mg_{30}O_{29}$ cluster. The first- and second- nearest neighbors of the O vacancy are emphasized with a small square, the third-, fourth- and fifth- with a large square. Definition of the geometrical parameters, Surface-Au distance (z_{S-Au}) and Au-Au distance (r_{Au-Au}). The two sets of equivalent distances R_1 and R_2 are also shown. The Mg, O and Au atoms are represented by gray, red and yellow circles respectively.

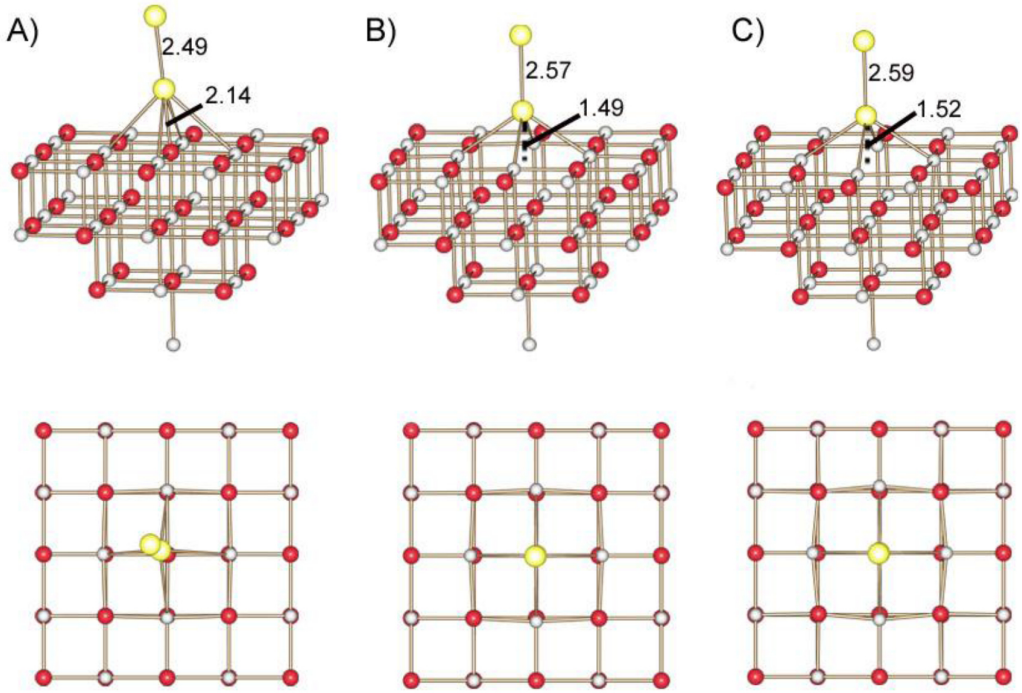

FIGURE 2. Lateral and top views of the optimized geometries of Au_2over and O_{5c} site (A), over an F_s color center (B), and over an F_s^+ color center (C) at the MgO(100) surface. The surface-Au (z_{S-Au}), and Au-Au distances (r_{Au-Au}) in units of Å are given for each case.

2. Methods

2.1. Cluster model

We discuss the theoretical model briefly; further details can be found in our previous work [27]. We have employed a cluster-embedding technique in which the active cluster $Au_2Mg_{30}O_{30}$ ($Au_2Mg_{30}O_{29}$) is treated within DFT calculations. An Evjen array [28] of 1740 point charges surrounds the active cluster to provide a proper electrostatic environment and boundary conditions, and to represent an MgO(100) surface with the Au_2 on top (Fig. 1A). The MgO(100) surface was initialized from the optimized rumpling and relaxation calculated previously [29,30], and a combination of equivalent and constrained optimization of selected surface atoms was performed [27]. In order to simulate the adsorption of the Au_2 particle on a regular oxygen site of the MgO surface, the all-electron $Mg_{30}O_{30}$ DFT cluster is initially centered on an O atom. To model the adsorption of Au_2 on F_s and F_s^+ color centers, we used $Au_2Mg_{30}O_{29}$ clusters with a neutral and single-charged oxygen vacancy at the center respectively.

TABLE I. The Surface-Au distance (z_{S-Au}) and Au-Au distance (r_{Au-Au}), BSSE corrected binding energies (E_a), dimerization energies (E_{dim} and E_b), and the NBO atomic charges for the absorption of Au_2 at the O_{5c}, F_s and F_s^+ sites. Two cases are shown, NN-free in which the surface atoms and Au_2 are optimized; and NN-frozen in which only the Au_2 was optimized. Au_I and Au_{II} are the gold atoms closer and more distant from the surface respectively. Results of previous studies are given for comparison.

Au_2 at	z_{S-Au}(Å)	r_{Au-Au} (Å)	E_a(eV)[a]	E_{dim} (eV)	E_b (eV)	Q(Au_I)	Q(Au_{II})
O_{5c}							
NN free	2.14	2.49	1.05 (1.88)	3.12	1.99	-0.01	-0.17
NN frozen	2.17	2.49	1.11 (1.75)	3.09	2.06	-0.03	-0.14
RPBE[15]			0.99				
PW91[17]	2.31	2.53	1.23				
PW91[18]	2.18	2.53	1.49	2.91	1.99		
PBE[21]	2.19	2.56	1.27 (1.61)				
F_s							
NN free	1.49	2.57	2.85 (4.05)	3.14	2.01	-0.66	-0.55
NN frozen	1.64	2.55	2.79 (3.65)	2.83	1.80	-0.62	-0.49
PW91[17]	1.60	2.59	3.72				
BP86[19,b]	1.62	2.63	4.06				
PBE[21]	1.69	2.62	3.38 (3.86)				
PW91[22]			3.57				
F_s^+							
NN free	1.52	2.59	1.93 (2.92)	1.29	0.16	-0.63	-0.02
NN frozen	1.67	2.58	2.05 (2.81)	1.39	0.36	-0.61	0.06
BP86[19]	1.62	2.60	2.40		-0.04		

We investigated two cases. First, the Au_2 dimer is fully optimized while the MgO surface is kept frozen denoted NN-frozen from here on. Second, the Au_2 and the first- and second- nearest neighbors of the Au_2-adsorption site on the MgO surface are fully optimized, while the third-, fourth-, and fifth- nearest neighbors are optimized only along the direction perpendicular to the surface, denoted NN-free from here on. For the third-, fourth-, and fifth- nearest neighbors we optimized two equivalent internal coordinates representing the bond length between an oxygen (magnesium) in the first cluster layer, and a magnesium (oxygen) on the surface, as shown in Fig. 1B.

2.2. Quantum chemical methods

All calculations were performed within the DFT formalism, and employed the Perdew, Burke, and Enzerhof generalized gradient approximation (GGA) [31]. The electronic orbitals and eigenstates were determined by using a linear combination of Gaussian atomic type orbital molecular orbital approach. The numerical calculations were carried out using the deMon2k software [32]. It uses variational fitting of the Coulomb potential to avoid the calculation of four-center electron repulsion integrals [33]. The exchange-correlation potential was calculated via numerical integration from the auxiliary function density [34]. All electrons of the MgO cluster were treated explicitly using the double-valence plus polarization (DZVP) basis sets (6321/411/1*) for magnesium and (621/41/1*) for oxygen [35]. For the gold atoms the relativistic effective core potential with 19 valence electrons proposed by Schwerdtfeger *et al.*, [36] in combination with the correlation consistent aug-cc-pVTZ-pp valence basis set [37] was used. The GEN-A2 auxiliary function set for Mg and O atoms, and the GEN-A2* set for the Au atoms were employed. For the geometry optimization, a quasi-Newton method in internal redundant coordinates was used [30,38]. This methodology has been used for the optimization of the rumpling and relaxation of the MgO(100) surface [29,30], and also has been shown to qualitatively reproduce the properties of the Au atom and dimer [27]. Additionally, we calculated the formation energy of the F_s site, as the energy required to remove an O atom in its triplet state from the MgO surface. Our calculated value of 9.01 eV is in excellent agreement with previous calculations employing both the embedded cluster method (9.07 eV, [39]) and plane wave basis sets (values of 9.02 eV [40] and 9.06 eV. [25]) The molecular geometries and orbitals were plotted with the Schakal [41] and Molden [42] software respectively. Natural bond orbital (NBO) charges [43] were determined at the optimized geometries to analyze the charge transfer from the MgO surface to the Au atoms.

3. Results and Discussion

3.1. Geometries of Au_2 and adsorption neighborhood

3.1.1. Au_2 on O_{5c}

Lateral and top views of the optimized geometry for the NN-free case for Au_2 adsorbed over an O_{5c}, F_s and F_s^+ sites on the MgO(100) surface are shown in Fig. 2. In the case of Au_2 adsorbed over an O ion (Fig. 2A) we found a small distortion of the surface at the adsorption site. The Mg ions (in gray) move away from the central O, while the O ions (second-nearest neighbors) do not move. The Mg ions are displaced from the bulk equilibrium position around 3.6% along the X and Y directions, and 1.8% in Z direction of the nearest neighbor bulk distance (X and Y directions are in the plane of the surface and Z direction begin perpendicular to the surface). The optimized R_1 and R_2 equivalent bond lengths that describe the position of the third-, fourth-, and fifth- nearest neighbors are 2.120 Å and 2.113 Å, close to the optimized value for the cluster model without the Au_2 unit, 2.121 Å and 2.106 Å respectively. This comparison shows that there is not a significant relaxation of the surface farther than the second neighbors of the absorption site. The Au_2 dimer was found almost perpendicular, to the surface; it was found deviated from the normal to the surface by 5.8°. The optimized surface-Au distance (z_{S-Au}) and the Au-Au distance (r_{Au-Au}) are 2.14 Å and 2.49 Å respectively (Fig. 2A). All these results are collected in Table I. The Au-Au distance is very close to the experimental value of 2.47 Å [44] for the Au_2 dimer showing that the MgO surface is not affecting the Au-Au bond. Table I also shows the results of the calcula tions with the surface frozen (NN-frozen). As expected from the small relaxation of the surface in the case of NN-free, z_{S-Au} and r_{Au-Au} were almost the same in both cases. For For comparison, we have also included the results of previous studies in Table I. As concluded in our previous work [27], 2.16 Å and 2.51 Å can be set as the upper limits for the z_{S-Au} and r_{Au-Au} distances respectively.

We also considered the case in which the Au_2 was optimized starting from an adsorption over an Mg site. In this case, the Au_2moved away from the Mg site toward an adjacent O atom, and the final geometry was very similar to the geometry of the Au_2 particle adsorbed over an O ion. We then performed an additional optimization in which movement of the Au_2 unit was allowed only in the direction perpendicular to the surface, and found a local minimum 1.21 eV higher in energy with respect to the case in which Au_2moved to an adjacent O site.

3.1.2. Au_2 on F_s (Vacancy with two electrons)

For Au_2 adsorbed over a neutral color F_s center, a substantial distortion of the surface near the $F_s$adsorption site is observed in the top view of the optimized geometry (Fig. 2B). Both the Mg ions (the F_s nearest neighbors) and the O ions (second-nearest neighbors) move away from the F_s site. The Mg ions are displaced from the bulk equilibrium position by around 6.4% in the X and Y directions and 0.1% in Z direction with respect to the nearest neighbor bulk distance of 2.105 Å, and the O ions are displaced from the bulk equilibrium position around 2.3% along the diagonal of the square formed by first- and second- nearest neighbors. The optimized R_1 and R_2 equivalent bond lengths are 2.120 Å and 2.111 Å respectively, again close to the optimized values for the cluster model without the Au_2 unit, 2.123 Å and 2.105 Å, just as in the case of the O_{5c} site. The optimized z_{S-Au} and r_{Au-Au} distances are 1.49 Å, and 2.57 Å respectively (Fig. 2B and Table I). The considerable reduction of z_{S-Au} with respect to the absorption on the O_{5c} site, the stretching of the r_{Au-Au} distance, and the distortion of the MgO surface near the F_s site all attest to the stronger interaction of the Au_2 with the surface at this absorption site.

The z_{S-Au} value of 1.64 Å obtained in the calculation with the surface frozen was found to be considerably larger (15 pm) than the value obtained with NN-free. Previous studies have reported values ranging from 1.60 to 1.69 Å (Table I). We believe that this discrepancy can be attributed to the sensitivity of the optimized z_{S-Au} distance with respect to the different models used to describe the absorption site. On the other hand, the r_{Au-Au}distance was more consistent with previous studies; here we can specify an upper limit of 2.59 Å for its value.

3.1.3. Au_2 on F_s^+ (Vacancy with one electron)

For Au_2 adsorbed over an F_s^+color center (Fig. 2C) the Mg ions (first-nearest neighbors) move away from the F_s^+ site by 8.3%, and the O ions (second-nearest neighbors) almost do not move, only 0.47% toward the color center, and 0.1% in the Z direction, with respect to the nearest neighbor bulk distance. The optimized R_1 and R_2 equivalent bond lengths are 2.121 Å and 2.110 Å respectively, again very close to the optimized values for the cluster model without the Au_2 unit of 2.122 Å and 2.109 Å. The z_{S-Au} and r_{Au-Au} optimized values are 1.52 Å and 2.59 Å respectively, see Fig. 2C and Table I. As in the case of the F_s site, we again found that the calculation with NN-frozen predicted a considerably larger z_{S-Au} of 1.67 Å. The value of r_{Au-Au} however, was not affected for the relaxation of the surface. A previous study [23] reported a z_{S-Au} value 1.62 Å intermediate between our NN-free and NN-frozen calculations.

3.2. Nature of the bonding, absorption energies, dimerization energies and charge transfer

To study the effect of the relaxation of the MgO surface on the absorption of the Au_2 dimer, we calculated the absorption and dimerization energies of Au_2 for both the NN-free and NN-frozen cases using the following equations:

$$E_a = E(Au_2) + E(\text{MgO site}) - E(Au_2\text{MgO site}),$$

$$E_{dim} = E(Au) + E(Au_1/\text{MgO site}) - E(Au_2/\text{MgO site}),$$

$$E_b = E(Au_1/MgO\ site) + E(Au_1/MgO\ O_{5c}) - E(Au_2/MgO\ site) - E(MgO\ O_{5c}).$$

Here $E(Au_2)$, E(MgO site), $E(Au_nMgO$ site), and E(Au) are the total energies for the optimized geometries of the respective clusters and of the Au atom. E_a is the absorption energy as corrected for the basis set superposition error (BSSE) using the counterpoise method [45]. We note that BSSE has been shown to be significant for the Au_nMgO systems with total energy differences of the order of 0.5 to 1 eV [25,27]. E_{dim} is the dimerization energy of a gas phase Au atom to another Au atom already bound to a given site (O_{5c}, F_s or F_s^+), and E_b is the binding energy of a Au atom bound to an O_{5c} site to another Au atom located on a given site (O_{5c}, F_s or F_s^+). According to the convention adopted in the equations above, E_a, E_{dim} and E_b are positive for a bound structure and larger values of E_{dim} and E_b imply enhanced structural stability of the Au_2 dimer.

3.2.1. *Au_2 on O_{5c}*

The calculated absorption energies for the NN-free and NN-frozen cases are very close, 1.05 and 1.11 eV respectively. These results are in agreement with previous studies that have reported values in the range of 0.99 to 1.27 eV [19,21,25]. Our calculated E_{dim} and E_b are respectively three and two times larger than E_a, thus showing that an adsorbed Au_2 will be stable toward dissociation (Table I). Further, the O_{5c} site will be expected to promote particle growth, particularly from an already absorbed Au atom and a gas phase Au atom, as the

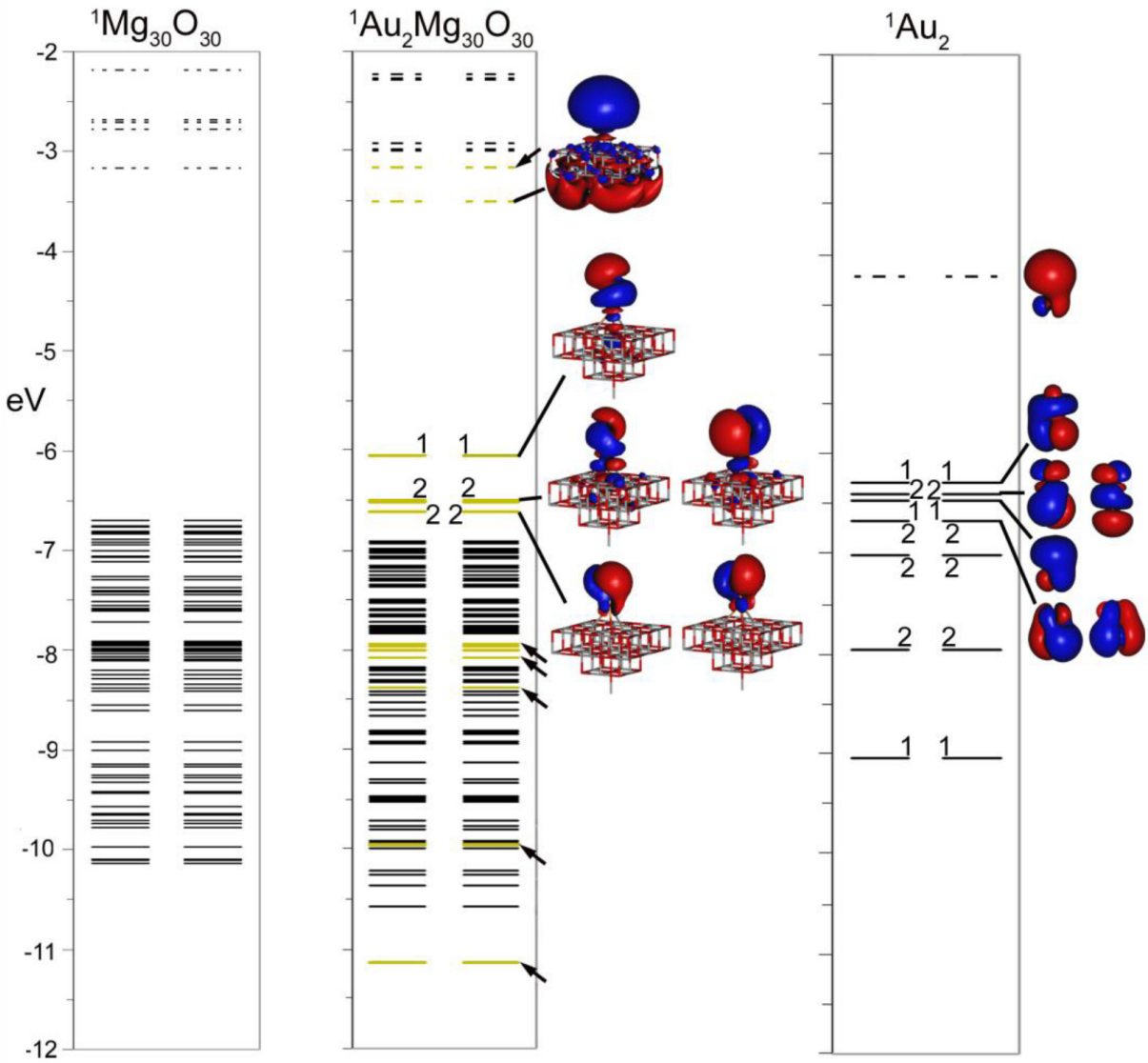

FIGURE 3. One electron energy levels and iso-surfaces (isovalue = 0.001 a.u.) of selected molecular orbitals of the $Mg_{30}O_{30}$, $Au_2Mg_{30}O_{30}$ and Au_2 clusters for NN-free. For $Au_2Mg_{30}O_{30}$ we have marked the energy levels with a significant contribution of the Au atoms with an arrow. The superscripts indicate spin multiplicity. The continuous lines represent occupied levels, the dotted lines correspond to single unfilled states, the degeneracy is marked next to selected levels, and both the majority (up) and minority (down) spin states are shown.

value of E_{dim} (3.12 eV) is larger than the experimental binding energy of two gas phase Au atoms (2.30 eV) [40].

To investigate the nature of the bonding of the Au_2at the O_{5c} site further, we plotted the one-electron energy levels and molecular orbital iso-surfaces for the optimized $Mg_{30}O_{30}$, $Au_2Mg_{30}O_{30}$, and Au_2 clusters for the NN-free case. These plots are shown in Fig. 3. The electronic configuration of Au is [Xe] $4f^{14}\ 5d^{10}\ 6s^1$, and an Au_2 molecule can accommodate 22 electrons (11 from each Au atom) in the eleven doubly occupied topmost energy levels. The lowest unoccupied molecular orbital (LUMO) of Au_2 is found to be 2 eV above the occupied states. After the binding of Au_2 with the $Mg_{30}O_{30}$ cluster, the five doubly occupied topmost energy levels of $Au_2Mg_{30}O_{30}$ accommodate 10 electrons from Au_2, and the remaining Au electrons form bonding states with the $Mg_{30}O_{30}$ cluster states that are located at lower energy, while the LUMO of Au_2 is pushed to higher energy. The energy levels with contributions from the Au atoms in $Au_2Mg_{30}O_{30}$ are marked with arrows in Fig. 3.

The catalytic properties of deposited gold clusters have been shown to depend substantially on the charge transfer from the surface to the cluster [6,13], and experimental studies by Sterrer *et al.* [46] have concluded that Au particles in color centers are negatively charged, while Au particles in regular terrace sites are neutral. Simic-Milosevic *et al.* [47] recently reported a combined experimental-theoretical study in which they found that Au_2 dimers on thin MgO(001) films grown on Ag(001) are neutral when absorbed in an upright position, and negatively charged when the dimer absorbs parallel to the surface. In the later case, the charge coming from the Ag(001) support populates the LUMO of Au_2. This result as well as the energy levels of Fig. 3 discussed above, can then explain why for the absorption of Au_2 on the F_s and F_s^+ sites of the MgO(001) surface, in which a charge transfer

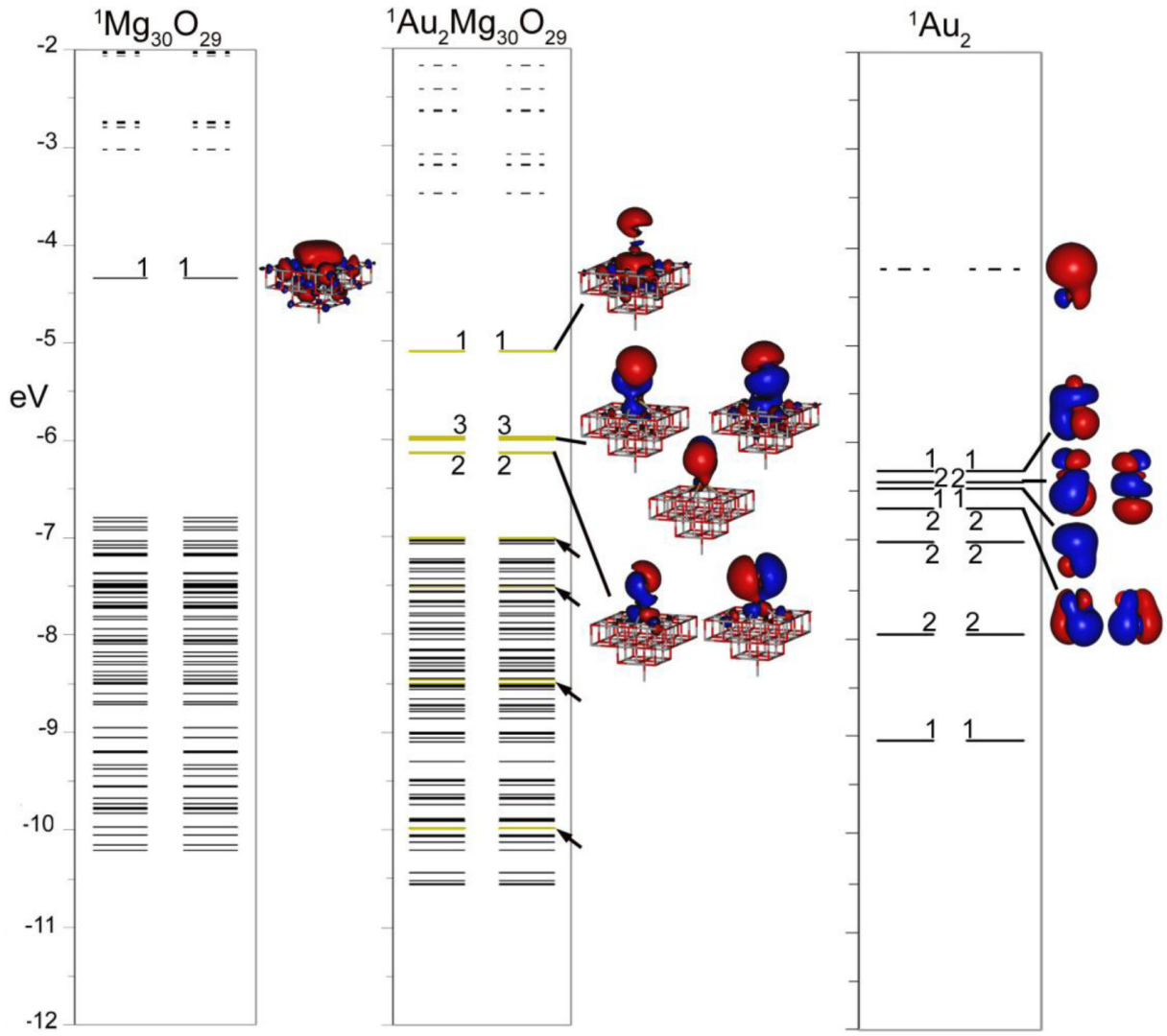

FIGURE 4. One-electron energy levels, and iso-surfaces of selected molecular orbitals of the $Mg_{30}O_{29}$, $Au_2Mg_{30}O_{29}$and Au_2 clusters for NN-free. See caption of Fig. 3 for more details.

exists, isomers with the Au_2 dimer tilted towards an Mg and an O atom have been predicted to be lower in energy than the vertical isomer [26,27].

In the present study we calculated NBO charges on the optimized geometries (Table I). Inspection of Table I shows that in both the NN-free and NN-frozen calculations, a small negative charge ($\sim$ 0.18 electrons) are located in the Au_2 dimer.

3.2.2. Au_2 on F_s (Vacancy with two electrons)

We found, as in the case of the O_{5c} site, similar values of E_a for both the NN-free and NN-frozen calculations (Table I). The E_a values are almost three times larger compared with those at the O_{5c} site. Although the NN-frozen calculations predicted a surface-Au distance 15 pm larger than the NN-free case, E_a values show only a small decrease from 2.85 eV for NN-free to 2.79 eV in the case of NN-frozen. The calculated E_{dim} and E_b however, presented differences of more that 0.20 eV, with the values calculated for NN-frozen being the smaller ones. Notably, previous reports have reported E_a values ranging from 3.38 to 4.06 eV [21,23,25-26] showing that E_a is sensitive to the model used to describe the absorption site.

To investigate the nature of the bonding of the Au_2at the F_s site, we plotted the one electron energy levels and molecular orbital iso-surfaces for the optimized $Mg_{30}O_{29}$, $Au_2Mg_{30}O_{29}$ and Au_2 clusters. These are shown in Fig. 4. Analysis of the energy levels of $Mg_{30}O_{29}$ shows that the two trapped electrons in the F_s site are located in the highest occupied molecular orbital (HOMO), and are considerably higher in energy compared to the rest of the energy levels. Interestingly, the LUMO of the Au_2 dimer is located at a similar energy (around -4 eV). The bonding interaction between these levels leads to strong binding, as attested by the high absorption energy and by the energy levels in Fig. 4. While the energy levels of the $Au_2Mg_{30}O_{29}$ cluster have a structure

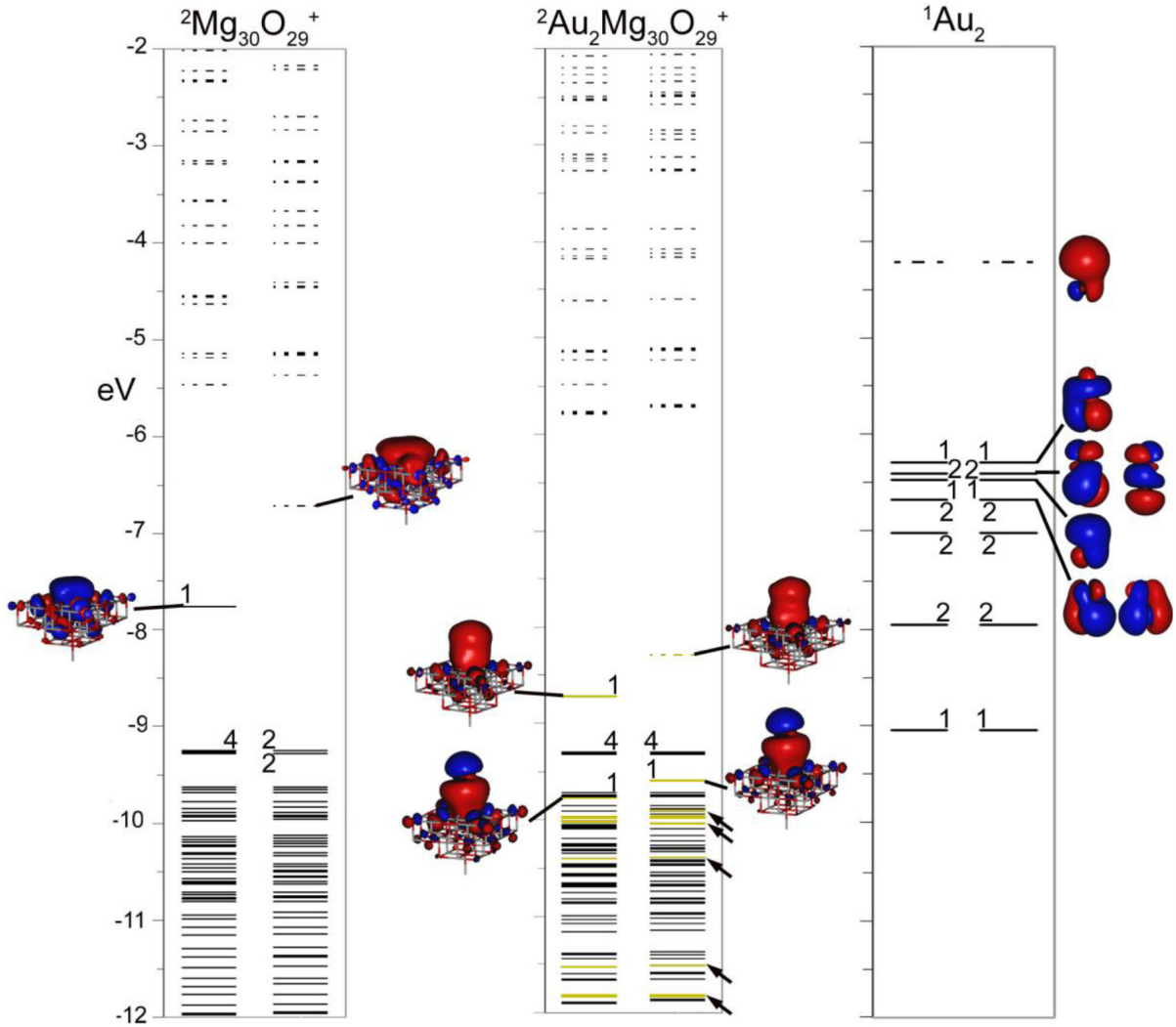

FIGURE 5. One-electron energy levels, and iso-surfaces of selected molecular orbitals of the $Mg_{30}O_{29}^+$, $Au_2Mg_{30}O_{29}^+$ and Au_2 clusters. See caption of Fig. 3 for more details.

similar to those of $Au_2Mg_{30}O_{30}$ (Fig. 3), in this case there is one more energy level, resulting in six doubly occupied topmost energy levels with predominant contributions form the Au atoms. An analysis of the charge transferred from the MgO surface to the Au_2dimer shows that there are respectively 1.21 and 1.11 electrons in $Au_2$for the case of the NN-free and NN-frozen calculations. In summary, the large values of E_a, E_b and E_{dim} indicate that the Au_2 dimer is strongly bonded and that the dimer can be formed either from two already absorbed Au atoms, or one absorbed and one gas phase Au atom.

3.2.3. Au_2 on F_s^+(Vacancy with one electron)

The calculated absorption energies for the case of the F_s^+ site are of the order of 2 eV and are similar for both the NN-free and NN-frozen cases. As in case of the F_s site, E_{dim} and E_b presented differences of 0.1 to 0.2 eV between both types of calculations (Table I). The small values of E_{dim}, 1.29 eV, and especially of E_b, 0.16 eV, imply that at this site once the dimer is absorbed it can dissociate easily, and thus F_s^+ is not a good nucleation site. Considering that the F_s^+ site has only one trapped electron, and that the Au atom is known to have a large electron affinity, a strong interaction of one Au atom at the F_s^+ site has been predicted. In fact, at this site, the Au atom presents the highest absorption energy of 3.39 eV, compared with only 0.60 and 2.53 eV for the O_{5c} and F_s sites respectively [23]. These factors explain the small values for the dimerization energies E_{dim} and E_b.

As for the other absorption sites, we investigated the one-electron energy levels and molecular orbital iso-surfaces for the optimized $Mg_{30}O_{29}^+$, $Au_2Mg_{30}O_{29}^+$, and Au_2 clusters, and are shown in Fig. 5. For the F_s^+ site, the absorption energy of Au_2 is almost two times larger compared with that at the O_{5c} site (Table I). An analysis of the energy levels of $Mg_{30}O_{29}^+$ shows that the trapped electron in the F_s^+ site interacts with the LUMO of the Au_2 dimer leading to a bonding interaction, and to an adsorption energy with a value intermediate between the ones for the O_{5c} and F_s sites. In the $Au_2Mg_{30}O_{29}^+$ cluster, the bonding energy levels of the Au_2 dimer are located lower in energy than the energy levels of $Mg_{30}O_{29}^+$, which are almost unaltered. An analysis of charge transfer from the MgO surface to the Au_2dimer shows that there are 0.67 and 0.65 electrons in $Au_2$for the case of NN-free and NN-frozen calculations. These values are half the ones found for the F_s site, and thus support our previous discussion.

4. Conclusions

We have analyzed the electronic and structural properties of the Au_2 dimer absorbed in a perpendicular configuration to the MgO(001) surface on a regular O_{5c} site and on the defect F_s and F_s^+ sites. We studied the two cases, in which the MgO(001) surface was relaxed and when it was frozen. For the O_{5c} site we found a small relaxation of the MgO surface upon Au_2 absorption, and thus the calculations for which the surface was kept frozen presented similar geometrical parameters, absorption and dimerization energies as those in which the surface was optimized.

For the F_s site a distortion of the surface in the neighborhood of the absorption site was observed. In this case the bonding of the Au_2 dimer to the surface can be explained from the bonding interaction between the doubly occupied HOMO of the $Mg_{30}O_{30}$ cluster that contains two trapped electrons in the F_s site, and the LUMO of Au_2. This bonding mechanism also explains the large calculated value of the charge transfer from the MgO surface to Au_2 and the highest absorption energy among the studied surface sites. The calculations with the MgO surface frozen predicted a considerably larger surface-Au distance (15 pm), as well as smaller dimerization energies ($\sim$ 0.2 eV) compared with the calculations where the MgO surface was allowed to relax.

For the F_s^+ site, a distortion of the surface in the neighborhood of the absorption site was observed. In this case the bonding mechanism is explained from the interaction between the single occupied HOMO of the $Mg_{30}O_{29}^+$ cluster and the LUMO of Au_2. This mechanism also explains why the charge transfer calculated from the MgO surface to Au_2 is only half the one calculated for the F_s site, and that the calculated absorption energy is intermediate between the O_{5c} and F_s sites. The calculations with the MgO surface frozen predicted a considerably larger surface-Au distance as in the case of the F_s site, and the dimerization energies differed by $\sim$ 0.15 eV compared with the calculations were the MgO surface was allowed to relax.

Acknowledgments

C.Q. acknowledges Prof. Dennis R. Salahub for valuable discussions. R.C and C.Q. acknowledge financial support by the PAPIIT-UNAM IN116912-3 project and Proyecto Universitario de Tecnología Ambiental PUNTA-UNAM. S.N.K. and J.U.R. acknowledges support from the MURI grant from the Air Force Office of Scientific Research grant. Part of the calculations was performed on the computational equipment of DGSCA UNAM, particularly at the super computer Kan-Balam.

1. A.F. Carley *et al.*, *Phys. Chem. Chem. Phys.* **13** (2011) 2528.
2. Z. Li, C. Ciobanu, J. Hu, J-P. Palomares-Baes, J-L. Rodrigez-Lopez and R. Richards, *Phys. Chem. Chem Phys.* **13** (2011) 2582.
3. I. Laoufit *et al.*, *J. Phys. Chem. C* **115** (2011) 4673.
4. W.H. Kim, K.H. Cho, K. Ch. Choi, D.Y. Kim, and O.O. Park, *IEEE Transactions on Electron Devices* **57** (2010) 2644.
5. M. Haruta, T. Kobayashi, H. Sano, and N. Yamada, *Chem. Lett.* **405** (1987).
6. A. Sanchez, S. Abbet, U. Heiz, W. Schneider, H. Hakkinen, R. Barnett, and U. Landman, *J. Phys. Chem. A* **103** (1999) 9573.
7. U. Heiz, A. Sanchez, S. Abbet, and W. Schneider, *Chem. Phys.* **262** (2000) 189.
8. M. Walter, and H. Hakkinen, *Phys. Rev. B.* **72** (2005) 205440.
9. L. Giordano, J. Carrasco, C. Di Valentin, F. Illas, and G. Pacchioni, *J. Chem. Phys.* **124** (2006) 174709.
10. M. Haruta, *Nature* **437** (2005) 1098.
11. N. Lopez, and J. Norskov, *J. Am. Chem. Soc.* **124** (2002) 11262.
12. M. Okumura, S. Tsubota, and M. Haruta, *J. Mol. Catal. A Chem.* **199** (2003) 73.
13. B. Yoon *et al.*, *Science* **307** (2005) 403.
14. S. Abbet, A. Sanchez, U. Heiz, W. Schneider, A. Ferrari, G. Pacchioni, and N. Rosch, *J. Am. Chem. Soc.* **122** (2000) 3453.
15. L. Giordano, C. Di Valentin, J. Goniakowski, and G. Pacchioni, *Phys. Rev. Lett.* **92** (2004) 096105.
16. A. Bogicevic, and D. Jennison, *Surf. Sci.* **515** (2002) L481.
17. Z.P. Liu, X.Q. Gong, J. Kohanoff, C. Sanchez, and P. Hu, *Phys. Rev. Lett.* **91** (2003) 266102.
18. X.Q. Gong, Z.P. Liu, R. Raval, and P. Hu, *J. Am. Chem. Soc.* **126** (2004) 8.
19. L.M. Molina, and B. Hammer, *Phys. Rev. B.* **69** (2004) 155424.
20. G. Pacchioni, L. Giordano, and M. Baistrocchi, *Phys. Rev. Lett.* **94** (2005) 226104.
21. G. Barcaro, and A. Fortunelli, *J. Chem. Theo. Comp.* **1** (2005) 972.
22. A. Del Vitto, G. Pacchioni, F. Delbecq, and P. Sautet, *J. Phys. Chem. B.* **109** (2005) 8040.
23. C. Inntam, L. Moskaleva, K. Neyman, V. Nasluzov, and N. Rosch, *Appl. Phys. A-Mater.* **82** (2006) 181.
24. Y. Chen, P. Crawford, and P. Hu, *Catal. Lett.* **119** (2007) 21.
25. R. Coquet, G. Hutchings, S. Taylor, and D. Willock, *J. Mater. Chem.* **16** (2006) 1978.
26. L. Molina, and J. Alonso, *J. Phys. Chem. C.* **111** (2007) 6668.
27. R. Caballero, C. Quintanar, A.M. Köster, S.N. Khanna, and J.U. Reveles, *J. Phys, Chem. C* **112** (2008) 14949.
28. H.M. Evjen, *Phys. Rev.* **39** (1932) 675.
29. C. Quintanar, R. Caballero, and V.M. Castaño, *Int. J. Quantum Chem.* **102** (2005) 820.
30. J.U. Reveles, S.N. Khanna, and A.M. Köster, *J. Mol. Struc.-Theochem* **762** (2006) 171.
31. J. Perdew, K. Burke, and M. Ernzerhof, *Phys. Rev. Lett.* **77** (1996) 3865.
32. A. M. Köster *et al*., *deMon2k, Ver. 2.3.6*(The deMon Developers, Cinvestav, México 2007). Available at http://www.deMon-software.com
33. J.W. Mintmire, and B.I. Dunlap, *Phys. Rev. A* **25** 88 (1982).
34. A.M. Köster, J.U. Reveles, and J.M. del Campo, *J. Chem. Phys.* **121** (2004) 3417.
35. N. Godbout, D.R. Salahub, J. Andzelm, and E. Wimmer, *Can. J. Chem.* **70** (1992) 560.
36. P. Schwerdtfeger, M. Dolg, W. Schwarz, G. Bowmaker, and P. Boyd, *J. Chem. Phys.* **91** (1989) 1762.
37. K. Peterson, and C. Puzzarini, *Theor. Chem. Acc.* **114** (2005) 283.
38. J.U. Reveles, and A.M. Köster, *J. Comput. Chem.* **25** (2004) 1109.
39. P. Sushko, A. Shluger, and C. Catlow, *Surf. Sci.* **450** (2000) 153.
40. A. Shluger, L. Kantorovich, A. Livshits, and M. Gillan, *Phys. Rev. B* **56** (1997 15332).
41. E. Keller, *Chem. Unserer Zeit* **14** (1980) 56. Available at http://www.krist.uni-freiburg.de/ki/Mitarbeiter/Keller/schakal.html
42. G. Schaftenaar and J. Noordik, *J. Comput. Aid. Mol. Des.* **14** (2000) 123. Available at http://www.cmbi.ru.nl/molden/molden.html
43. E. Glendening *et al.*, *Theoretical Chemistry Institute*, (University of Wisconsin, Madison, WI, 2004); http://www.chem.wisc.edu/∼nbo5.
44. M. Morse, *Chem. Rev.* **86** (1986) 1049.
45. S. Boys and F. Bernardi, *Mol. Phys.* **100** (2002) 65.
46. M. Sterrer *et al.*, *Angew. Chem. Int. Edit.* **45** (2006) 2630.
47. V. Simic-Milosevic *et al.*, *J. Am. Chem. Soc.* **130** (2008) 7814.